# Supporting Information

Farver et al. 10.1073/pnas.1215081110

## SI Text

### Analysis of Averaged B Factors of Selected Residues

In a high-quality 3D protein model, B factors reflect the mobility or flexibility of various parts of the molecule. High B factors mean greater uncertainty about the actual atom position; e.g., they may imply disorder (free movement of a side chain or alternative side-chain conformations). We have included an analysis of average B factors for the ligand loops, from Asn42 to Asn47 and from Phe110 to Lys122, which contain all the interactions among the copper ion, ligands, and residues around them. Although not all mutants crystallize in the exact same space groups, most are in the p21 or closely related space groups (e.g., p21 for Asn47Ser/Phe114Asn vs. p212121 for Phe114Pro and Asn47Ser/ Met121Leu). Therefore, to compensate for this variance among the datasets, we have normalized the B-factor analysis relative to the entire protein structure. Because protein–protein (packing) interactions, temperature variance, and solvent effects should affect the entirety of the structure in a global sense, the normalization should achieve a reasonable scaling of the B factors of the critical ligand binding loops so that they may be compared on a similar basis. Table S5 contains a $B_{loop}/B_{TOT}$ column. A higher $B_{loop}/B_{TOT}$ ratio would correspond to a loop that is less stable relative to the entire structure.

### Analysis of Electron Paramagnetic Resonance Data and Its Implication for the Electronic Coupling

Calculations based on Eq. **4** in ref. 1,

$$A_{\parallel} = P_d\left\{\left(-\kappa - \frac{4}{7}\right)\alpha^2 + \frac{3}{7}(g_{\perp} - 2.00) + \left(g_{\parallel} - 2.00\right)\right\},$$

were carried out using $P_d = 396 \times 10^{-4}$ cm$^{-1}$ (1). $\kappa$ is the Fermi contact, and $\alpha^2$ is the percent metal character in the Cu($3d_{x2\text{-}y2}$) orbital. The resultant calculation of the first term in brackets on the right side of the equation (including both $\kappa$ and $\alpha^2$, with opposite sign) is presented in Table S2 as the "Fermi contact term." Assuming $\kappa$ is constant, there is slightly more Cu($3d_{x2\text{-}y2}$) character in the Asn47Ser/Phe114Asn and in Asn47Ser/Phe114Asn/Met121Leu mutants. However, the electron transfer (ET) rate constant of the former is higher than the maximum of the Marcus curve (Fig. 2), whereas the latter exhibits the smallest ET rate. Further, for the mutants in which covalency was measured (1), the highest degree of covalency is observed for Phe114Pro, which nevertheless displays a rate constant that fits the theoretical curve (Fig. 2). Thus, the small differences in anisotropic covalency observed among the mutants apparently have only a minor effect on the total electronic coupling along the ET pathway from electron donor to acceptor. Calculation of the exponential decay constant, $\beta$, is based on the scatter of the data presented Fig. 2 to explain the deviation between the experimental rate constants and the Marcus curve. Values of $\beta$ larger than 10.0 indicate experimentally determined rate constants below the theoretical curve, and $\beta$ values smaller than 10.0 indicate rate constants above the curve (Fig. 2). An average $\beta = 10.0 \pm 0.2$ nm$^{-1}$ is found.

### Calculation of Reorganization Energies, $\lambda_{calc.}$, for Each Mutant from Their Activation Parameters

The activation free energies, $\Delta G^*$ of the ET reactions in each mutant have been calculated from the respective activation parameters presented in Table S1. However, the entropy of activation determined experimentally, $\Delta S^{\ddagger}$, includes a contribution from the electronic coupling (equations 36c and 33b in ref. 2):

$$\Delta S^{\ddagger} = \Delta S^* + R\ln(\kappa\nu/10^{13}) = \Delta S^* - R\beta(r - r_0),$$

where $R$ is the gas constant (missing in equation 36c in ref. 2).

Using $\beta(r - r_0) = 23.8$, we obtain $R\beta(r - r_0) = 198$ JK$^{-1}$·mol$^{-1}$ (or 2.05 meV·K$^{-1}$). We then calculate $\Delta G^*$ (see Table S4) using the activation enthalpy and the corrected activation entropy values. Finally, the reorganization free energy, $\lambda_{calc.}$, is calculated using equation:

$$\Delta G^* = \frac{\lambda}{4}\left(1 + \frac{\Delta G^0}{\lambda}\right)^2.$$

The $\lambda_{calc.}$ values presented in the last column of Table S4 are seen to fit very well with $\lambda_{TOT}$ determined using Eqs. **1** and **2** in the main text. Table S4 demonstrates a significant trend in the values of the activation free energies: Upon an increase in driving force ($-\Delta G^0$) (from the left to the right side of the barrier; compare with Fig. 2), the activation free energies $\Delta G^*$ decrease from 0.033 eV to very small numbers, reflecting the vanishing barriers, followed by an increase back to 0.040 eV for the last (triple) mutant (Asn47Ser/Phe114Asn/Met121Leu). The fluctuations probably reflect the accuracy of the numbers involved.

1. Hadt RG, et al. (2012) Spectroscopic and DFT studies of second-sphere variants of the type 1 copper site in azurin: Covalent and nonlocal electrostatic contributions to reduction potentials. *J Am Chem Soc* 134(40):16701–16716.

2. Marcus RA, Sutin N (1985) Electron transfers in chemistry and biology. *Biochim Biophys Acta* 811:265–322.

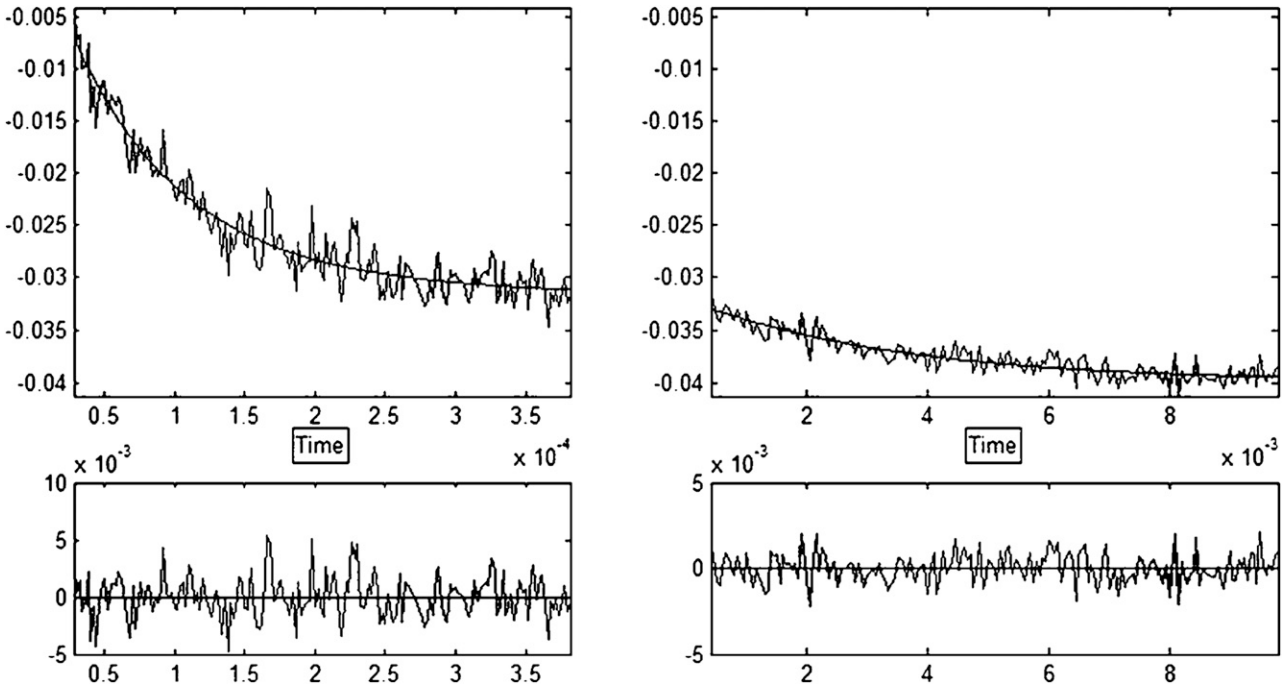


**Fig. S1.** Time-resolved absorption changes monitored at 635 nm of an Asn47Ser/Met121Leu azurin (Az) solution subjected to radiation pulses, illustrating reduction of Cu(II). The protein concentration was 106 μM in an anaerobic $N_2O$ saturated solution. The time scale is in seconds. All other technical details have been described in *Methods*.

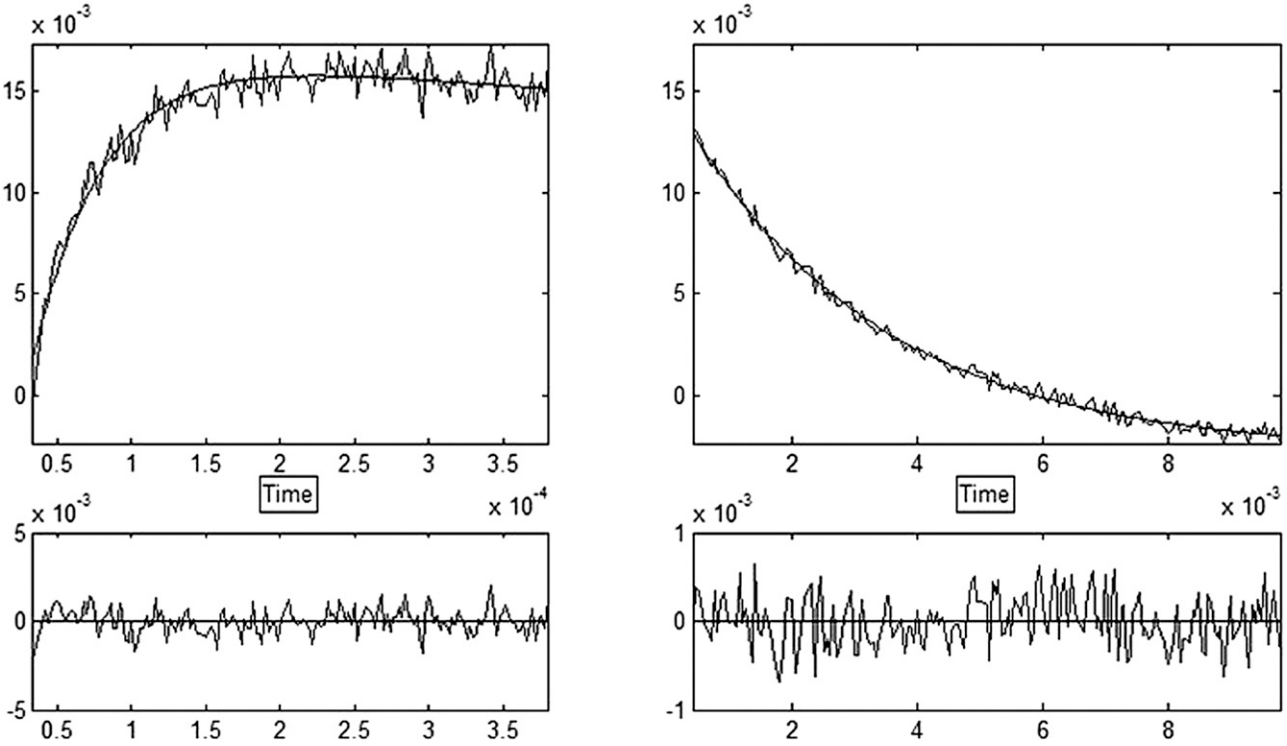


**Fig. S2.** Time-resolved absorption changes monitored at 410 nm of an Asn47Ser/Met121Leu Az solution subjected to radiation pulses, illustrating formation and decay of the disulfide radical ions. All other details are described in the Fig. S1 legend.

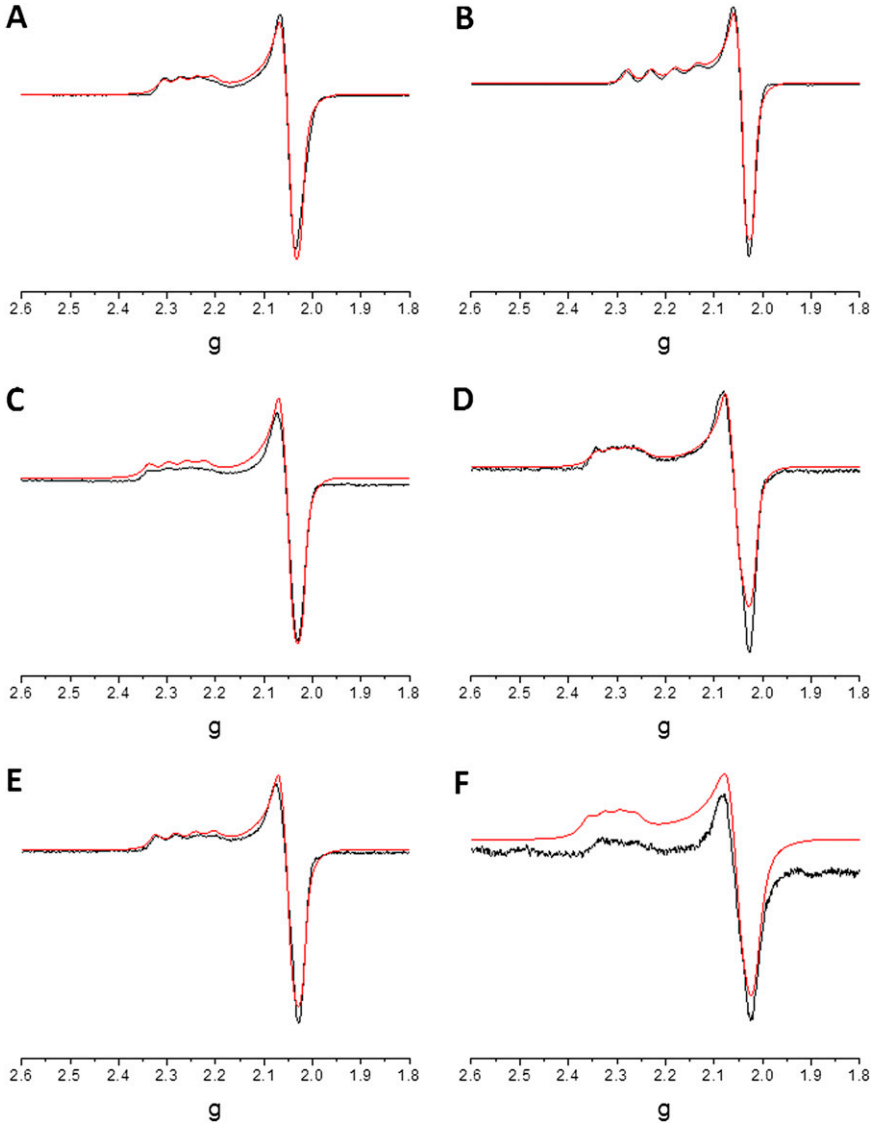


**Fig. S3.** Electron paramagnetic resonance data for (*A*) Phe114Pro/Met121Gln, (*B*) Phe114Pro, (*C*) Asn47Ser/Phe114Asn, (*D*) Asn47Ser/Met121Leu, (*E*) Phe114Asn/Met121Leu, and (*F*) Asn47Ser/Phe114Asn/Met121Leu Az. Experimental spectra are shown in black and simulations in red.

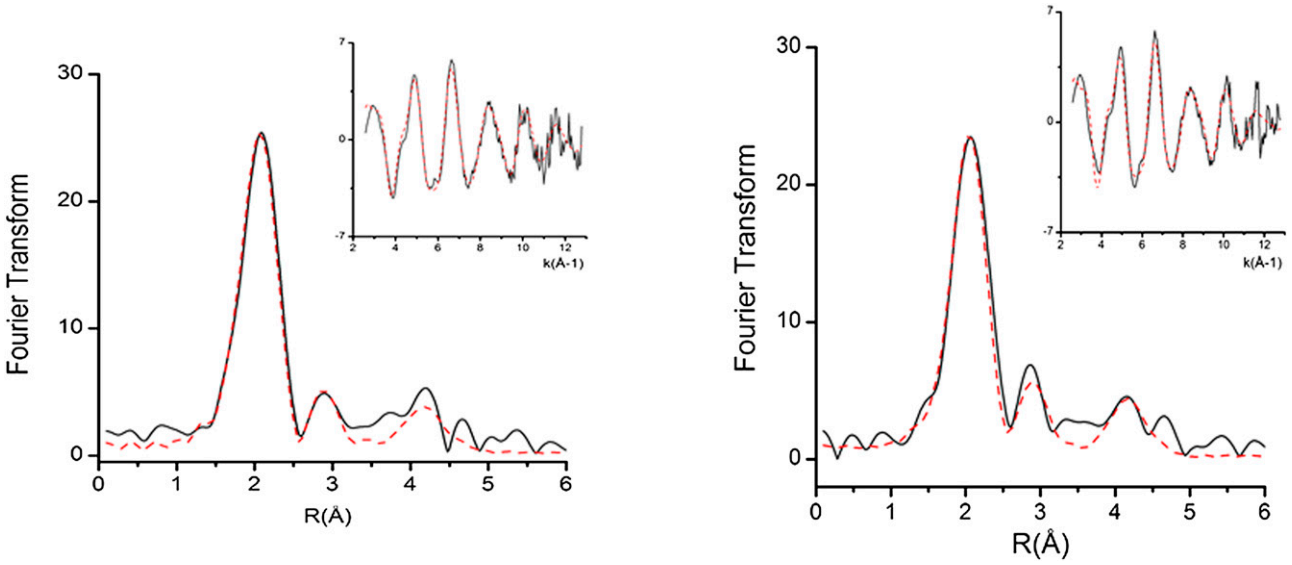


**Fig. S4.** Fourier transform and extended X-ray absorption fine structure (EXAFS; *Inset*) for WT Az (*Left*) and Asn47Ser/Phe114Asn/Met121Leu Az (*Right*). Experimental data are shown as solid black lines and simulations as dashed red lines.

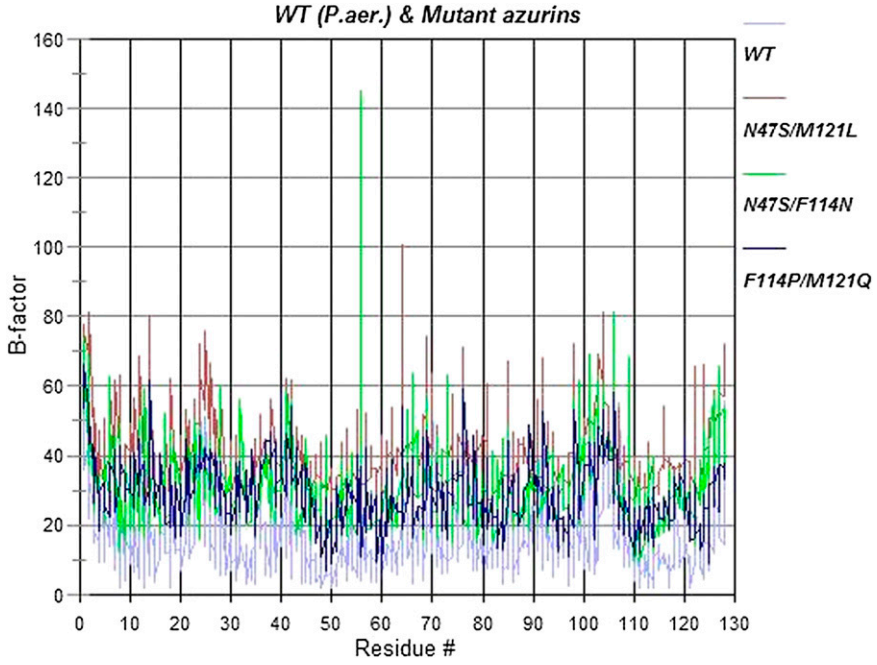


**Fig. S5.** Plot of B factors for the individual residues in WT and mutant Az; compare with Table S5.

**Table S1. Rate constants and activation parameters**

| Az mutant | $k_{ET}$, $s^{-1}$ at 298 K | Reduction potential, mV (1) | $\Delta H^{\ddagger}$ kJ·mol$^{-1}$ | $\Delta S^{\ddagger}$ J·K$^{-1}$·mol$^{-1}$ |
|---|---|---|---|---|
| Phe114Pro/Met121Gln | 81 ± 11 | 114 ± 49 | 36.6 ± 7.5 | −86 ± 14 |
| Phe114Pro | 191 ± 26 | 219 ± 8 | ∼29 | −106 |
| Asn47Ser/Phe114Asn | 387 ± 59 | 490 ± 12 | 33.7 ± 2.5 | −82 ± 4 |
| Asn47Ser/Met121Leu | 355 ± 51 | 509 ± 3 | 44.0 ± 2.1 | −48 ± 1 |
| Phe114Asn/Met121Leu | 287 ± 34 | 535 ± 11 | ∼39 | ∼ −66 |
| Asn47Ser/Phe114Asn/Met121Leu | 78 ± 12 | 641 ± 9 | 41.7 ± 5.9 | −71 ± 8 |
| WT *P. aeruginosa* (2) | 44 ± 7 | 286 ± 8 | 47.5 ± 2.2 | −56 ± 4 |
| Cys112Asp (3) | 123 | 180 | 34.8 ± 4.0 | −88 ± 8 |
| Cys112Asp/Met121Leu (3) | 61 | 281 | 22.6 ± 1.0 | −135 ± 4 |

1. Marshall NM, et al. (2009) Rationally tuning the reduction potential of a single cupredoxin beyond the natural range. *Nature* 462(7269):113–116.
2. Farver O, Pecht I (2011) Electron transfer in blue copper proteins. *Coord Chem Rev* 255(7-8):757–773.
3. Lancaster KM, et al. (2011) Electron transfer reactivity of type zero Pseudomonas aeruginosa azurin. *J Am Chem Soc* 133(13):4865–4873.

**Table S2. EPR parameters of the Az mutants for which intramolecular ET has been studied together with calculated Fermi contact terms and exponential decay constants, β**

| Parameters | WT | Phe114Pro/ Met121Gln | Phe114Pro | Asn47Ser/ Phe114Asn | Asn47Ser/ Met121Leu | Phe114Asn/ Met121Leu | Asn47Ser/ Phe114Asn/ Met121Leu |
|---|---|---|---|---|---|---|---|
| $g_x$ | 2.028 | 2.030 | 2.028 | 2.028 | 2.026 | 2.028 | 2.021 |
| $g_y$ | 2.055 | 2.054 | 2.049 | 2.056 | 2.062 | 2.057 | 2.058 |
| $g_z$ | 2.262 | 2.257 | 2.205 | 2.280 | 2.298 | 2.263 | 2.310 |
| $A_x$ /cm$^{-1}$ | $8.5 \times 10^{-4}$ | $7.9 \times 10^{-4}$ | $7.0 \times 10^{-4}$ | $8.9 \times 10^{-4}$ | $9.6 \times 10^{-4}$ | $8.7 \times 10^{-4}$ | $9.2 \times 10^{-4}$ |
| $A_y$/cm$^{-1}$ | $8.6 \times 10^{-4}$ | $7.9 \times 10^{-4}$ | $7.0 \times 10^{-4}$ | $8.9 \times 10^{-4}$ | $9.6 \times 10^{-4}$ | $8.7 \times 10^{-4}$ | $9.2 \times 10^{-4}$ |
| $A_z$/cm$^{-1}$ | $5.3 \times 10^{-3}$ | $4.5 \times 10^{-3}$ | $6.5 \times 10^{-3}$ | $5.0 \times 10^{-3}$ | $3.9 \times 10^{-3}$ | $5.3 \times 10^{-3}$ | $4.2 \times 10^{-3}$ |
| Fermi contact term | 0.414 | 0.389 | 0.386 | 0.424 | 0.415 | 0.415 | 0.433 |
| β/nm$^{-1}$ | — | 10.08 | 9.92 | 9.84 | 9.88 | 9.84 | 10.17 |

Electron paramagnetic resonance (EPR) spectra were measured under conditions identical to those of the ET measurements.

**Table S3. EXAFS analysis for WT and Asn47Ser/Phe114Asn/Met121Leu Az**

| | | Cu–S | | | Cu–N(His) | | | |
|---|---|---|---|---|---|---|---|---|
| Sample/fit | F | N | R, Å | DW, Å$^2$ | N | R, Å$^2$ | DW, Å | $E_0$ |
| WT (oxidized) | 0.510 | 1 | 2.17 | 0.003 | 2 | 1.93 | 0.008 | −2.346 |
| Asn47Ser/Phe114Asn/ Met121Leu oxidized | 0.580 | 1 | 2.17 | 0.008 | 2 | 1.95 | 0.013 | −2.905 |

DW, Debye-Waller factor; $E_0$, inner shell binding energy; F, fit; N, number of bonds; R, bond length.

**Table S4. Determination of reorganization free energies, $\lambda_{calc.}$, for the individual mutants**

| Mutant | $-\Delta G^0$ eV | $\Delta G^*$ eV | $\lambda_{calc.}$ eV |
|---|---|---|---|
| Phe114Pro/Met121Gln | 0.491 ± 0.196 | 0.033 ± 0.007 | 0.82 |
| Phe114Pro | 0.629 ± 0.023 | ~0.016 | 0.86 |
| Asn47Ser/Phe114Asn | 0.900 ± 0.022 | −0.009 ± 0.001[a] | 0.90 |
| Asn47Ser/Met121Leu | 0.919 ± 0.005 | −0.007 ± 0.006[a] | 0.92 |
| Phe114Asn/Met121Leu | 0.945 ± 0.019 | ~ −0.003[a] | 0.94 |
| Asn47Ser/Phe114Asn/ Met121Leu | 1.051 ± 0.015 | 0.040 ± 0.006 | 0.71 |
| WT *P. aeruginosa* | 0.696 ± 0.020 | 0.054 ± 0.003 | 1.21 |

[a]For the small negative values in the third column, we use $\Delta G^* = 0$ to calculate $\lambda_{calc.}$. The average value of $\lambda_{calc.}$ for the mutants from the last column is 0.86 ± 0.09 eV, in very good agreement with the value found from the fitting in Fig. 2: $\lambda_{TOT} = 0.81$ (+0.07/−0.05) eV.

**Table S5. Averaged B factors for WT and mutated azurins calculated from their respective PDB files**

| Protein | PDB file | $B_{TOT}$, Å$^2$ | $B_{42–47}$, Å$^2$ | $B_{42–47}/B_{TOT}$ | $B_{110–122}$, Å$^2$ | $B_{110–122}/B_{TOT}$ | $B_{Cu}$, Å$^2$ | $B_{Cu}/B_{TOT}$ | Resol., Å | Temp., K |
|---|---|---|---|---|---|---|---|---|---|---|
| WT | | | | | | | | | | |
| *Pseudomonas aeruginosa* | 4AZU | 16.7 | 10.2 | 0.613 | 9.5 | 0.57 | 10.7 | 0.641 | 1.9 | 277 |
| Mutants | | | | | | | | | | |
| Asn47Ser/ Met121Leu | 3JT2 | 40.5 | 37.8 | 0.933 | 34.7 | 0.857 | 29.4 | 0.726 | 2.1 | 100 |
| Asn47Ser/ Phe114Asn | 3JTB | 31.1 | 28.4 | 0.915 | 25.5 | 0.820 | 24.8 | 0.797 | 1.8 | 100 |
| Phe114Pro | 2GHZ | 16.9 | 14.4 | 0.856 | 15.7 | 0.927 | 15.2 | 0.899 | 1.6 | 100 |
| Phe114Pro/ Met121Gln | 3INO | 28.9 | 31.6 | 1.09 | 23.9 | 0.827 | 25.2 | 0.872 | 2.3 | 100 |
| Cys112Asp/ Met121Leu | 3FPY | 26.2 | 21.6 | 0.824 | 19.1 | 0.729 | 23.8 | 0.908 | 2.1 | 100 |
| Cys112Asp | 3FQY | 26.4 | 22.2 | 0.842 | 22.4 | 0.846 | 25.4 | 0.960 | 1.9 | 100 |

PDB, Protein Data Bank; Resol., resolution; Temp., temperature.